Original paper

Folia Neuropathologica

Mechanism of RNA-binding protein Lin28 in neuronal ferroptosis after intracerebral haemorrhage

Luqian Feng, Likun Wang, Guofeng Wu

Clinical College, Guizhou Medical University, Guiyang, Guizhou, China

Folia Neuropathol 2022; 60 (1): 35-47 *DOI: https://doi.org/10.5114/fn.2022.114101*

Abstract

Intracerebral haemorrhage (ICH) is a highly risky cerebrovascular disease with poor prognosis. Lin-28 homolog A (Lin28) has been identified as a crucial regulator in ICH. This study aims to analyse the mechanism of Lin28 in neuronal ferroptosis after ICH and provide theoretical basis for ICH treatment. An ICH mouse model was established via injection of collagenase VII, followed by neurological impairment assessment, and haematoxylin-eosin staining. An in vitro ICH model was established using hemin treatment. Next, cell viability and ferroptosis parameters were detected via cell counting kit-8, assay kits, enzyme-linked immunosorbent assay and western blot. Lin28 expression and tripartite motif-containing 37 (Trim37) mRNA level were detected via western blot and quantitative real-time polymerase chain reaction (qRT-PCR). The binding relationship of Lin28 and Trim37 was verified. ICH mice exhibited neuronal ferroptosis and upregulation of Lin28. Lin28 inhibition alleviated neurological impairment, manifested by decreased hematoma, oedema, neuronal necrosis, glial cell swelling, intracellular vacuoles and inflammatory cell infiltration, reduced Fe^{2+} concentration and reactive oxygen species content, and increased glutathione and glutathione peroxidase 4 activity. In the hemin-induced HT-22 cells, Lin28 inhibition promoted cell viability and alleviated neuronal ferroptosis. Lin28 bound to Trim37 mRNA to stabilize the mRNA level of Trim37. Overexpression of Trim37 reversed the alleviating role of silencing Lin28 in neuronal ferroptosis after ICH. Overall, Lin28 stabilized the mRNA level of Trim37 to aggravate neuronal ferroptosis after ICH.

Key words: *RNA-binding proteins, LIN28, intracerebral haemorrhage, Trim37, ferroptosis, neurons.*

Introduction

Intracerebral haemorrhage (ICH) is a lethal form of stroke (accounting for 10% to 20% cases), diagnosed as an event of brain parenchymal bleeding after arteriole angiorrhexis [7,35]. Histopathologically, ICH is featured by formation of hematoma and oedema, white matter injury and neuron death in the inflammatory environment [11]. The clinical therapies for ICH patients mainly aim to reverse intracranial pressure and systemic hypertension and retard hematoma expansion [35]. Unfortunately, the theoretical basis for ICH treatment remains unsubstantial and targeted methods are urgent to be investigated to fight against clinical nihilism [22]. Ferroptosis is identified as a novel mode of iron-dependent cell programmed death, resulting from the triumph of the oxidant system over the antioxidant system, which leads to overproduction of reactive oxygen species (ROS), iron accumulation, lipid peroxidation and changes of other relevant cytokines [24]. Extensive evidence has proved that ferroptosis

Communicating author

Guofeng Wu, Clinical College, Guizhou Medical University, No. 28 Guiyi Street, Guiyang, 550004, Guizhou, China, phone: 13809431723, e-mail: drwuguofeng@163.com

serves as a major contributor to neuronal death and neurological impairment after ICH [1,26]. Nevertheless, the underlying mechanism of ferroptosis and its specific agencies in ICH need to be further investigated in detail.

RNA-binding proteins (RBPs) serve as critical molecules that participate in regulation of gene expression in multiple diseases by mediating stability messenger RNA (mRNA) [23]. Lin-28 homolog A (Lin28) as an RBP regulates the cell life-cycle *via* manipulation of mRNA stability, such as proliferation, apoptosis, differentiation and so on [16,19,21]. Lin28 upregulation plays a suppressive role in neurogenesis and neurite outgrowth which are related to adverse outcomes after ICH [3,33]. Essentially, Lin28 has been noted to have an aberrant expression in neurons after ICH and motivate astrocytic proliferation in pathogenesis of ICH [5]. Nevertheless, the mechanism of Lin28 in neuronal ferroptosis and regulation of mRNA stability after ICH remains elusive.

Tripartite motif (Trim) family proteins, a subtype of E3 ubiquitin ligases, are well known for their properties in a myriad of cellular activities and carcinogenesis [10]. Those proteins are also associated with an increased risk of brain neuronal injury. For instance, absence of TRIM8, Trim14 and Trim47 was demonstrated to quench inflammation and apoptosis in cerebral injury [2,9,29]. In this study, we uncovered the binding of Lin28 and Trim containing protein 37 (Trim37) mRNA through database prediction and relevant assays. Trim37 has been found to be elevated in serum of ICH patients and its inhibitor is potent to suppress inflammatory responses and microglial cell apoptosis after ICH [8]. Yet, the role of the Lin28-mediated Trim37 axis in neuronal ferroptosis has not been researched before.

Based on the aforementioned findings as we reviewed the literature, we speculated that Lin28 could bind to Trim37 mRNA to regulate Trim37 expression, thus affecting neuronal ferroptosis ICH, and the study is designed to confirm the therapeutic role of the Lin28 in ICH treatment.

Material and methods

Ethics statement

The animal experimentation is conducted in accordance with the protocol approved by the animal ethics committee of the Guizhou Medical University, and strictly followed the Guidelines for the Care and Use of Laboratory Animals [14].

Experimental animals and animal model

C57BL/6 mice (Wuhan University Centre for Animal Experiments, Approval No: SCXK (Hubei) 2019-0004) (n = 6, aged 8-10 weeks, weighing 25-28 g) had free access to clean food and water at 24ºC with relative humidity of 60%, and under a 12-h light/dark cycle. Lentiviral vectors were stereotactically injected into mouse brains. Briefly, mice were fixed using a stereotaxic apparatus (Render Biotech Co., Ltd, Shenzhen, China) and the head skin was sterilized using iodophor. The bregma was set as the original point (anteroposterior [AP] = 0 mm, mediolateral [ML] = 0 mm, dorsoventral [DV] = 0 mm). The 2.0 µl (10^8-10^9 TU/ml) lentiviral vectors (LV-sh-Lin28 or LV-sh-NC) were injected into mouse hippocampus (AP = –2.0 mm, ML = ±1.5 mm, DV = –1.6 mm) at the injection rate of 0.2 µl/min. After injection, the needle was indwelled for 5 min to avoid fluid reflux, followed by suture of the wound and disinfection with iodophor. At 72 h after injection of lentiviral vectors, mice were anesthetized using intraperitoneal injection of 2% pentobarbital sodium (40 mg/kg) and kept in the prone position on the stereotaxic apparatus (Render Biotech). A burr hole with a diameter of 1 mm (2.0 mm lateral to the bridge bone, 3.5 mm below the craniofacial surface) was drilled using a dental drill. Mice in the model group were injected with 0.1 U collagenase IV dissolved in 1 µl normal saline (NS) into the hole at the rate of 0.2 µl/min to induce ICH. The drill was left for 10 min to avoid fluid reflux and removed at the rate of 1 mm/min. Mice in the sham group were treated with the equal volume of NS. After surgery, mice were placed on the heating pad at 25°C to prevent hypothermia during recovery.

Neurological function deficit score

At 3 days after modelling, neurological function deficit was scored according to the method described in the prior literature [27] to reflect motor, sensory, reflex, and balance functions. The neurological impairment was assessed using the 18 score-mNSS system, including motor, sensory, reflex, and balance tests. The tests were graded from score 0 to score 18, with a higher score indicating a more severe neurological impairment. Besides, the scores

were evaluated by two technicians who were blind to the groups of mice.

Forelimb placing and corner turn tests

To assess neurological functions in a comprehensive manner, mice were subjected to forelimb placing and corner turn tests. The forelimb placing test was performed to assess the motor and sensory capacity. The mice were held to make forelimbs hang in the air and mouse tentacles were stimulated to assess the success rate of mouse forelimb placing on the table. In terms of the corner turn test, mice were placed at 30°-angled corner and the times of left/right turn to get out of the corner were recorded. The percentage of turning direction = left turns/total turns × 100%. The tests were performed in a double-bind manner.

Acquisition of blood and tissue specimens

At 3 days after modelling, 1 ml whole blood was collected from mouse eyeballs for preparation of the serum specimen, left for 40 min and then centrifuged at 1000 g for 10 min. The obtained serum specimens were restored in a refrigerator at –80°C for the detection of glutathione (GSH) and ROS in the serum. After blood acquisition, mice were euthanatized by an injection of 200 mg/kg pentobarbital sodium, followed by collection of brain tissues. The brain tissues of 6 mice in each group were randomly selected and frozen at –20°C for 30 min to make the cranial coronal plane at a thickness of 1 mm for hematoma measurement. The brain tissues of another 6 mice in each group were fixed in 4% paraformaldehyde solution for 24 h and embedded in paraffin after dehydration. The paraffined blocks were cut into sections at a thickness of 5 µm for haematoxylin-eosin (H&E) staining. The brain tissues of remaining 6 mice in each group were used to make tissue homogenate.

Brain oedema measurement

At 3 days after modelling, brain water content was measured according to the wet-dry weight ratio of brain tissues. The brain tissues were weighed immediately after mouse death on an electronic balance, which was recorded as wet weight. Then, brain tissues were dried at 68°C for 48 h and weighed as the dry weight. Brain oedema was calculated as follows: (wet weight – dry weight)/wet weight × 100%.

Brain hematoma measurement

The hematoma area of brain tissues was determined using the Image-Pro Plus 5.0 image processing software (National Institutes of Health, Bethesda, Maryland, USA). The hematoma volume was calculated in accordance to the following formula: $V = t \times (A1 + A2 + \cdots + An)$, where V – hematoma volume, t – slice thickness, A – hematoma area.

H&E staining

Mouse brain tissues were stained with haematoxylin-eosin and then photographed using the Image-Pro Plus 5.0 image processing software (National Institutes of Health, Bethesda, Maryland, USA).

Iron content measurement

The mouse brain tissue homogenate and HT-22 cells were washed with phosphate buffer saline (PBS) twice and then the content of Fe^{2+} was measured according to the instruction of iron content assay kits (R&D System, Inc., Minneapolis, MN, USA). The absorbance at the wavelength of 593 nm was determined and the standard curve was graphed for measurement of iron content. The experiment of each group was performed in triplicate.

Cell culture and treatment

Mouse hippocampal neuronal cell line HT-22 cells (Cell Bank of Chinese Academy of Sciences, Shanghai, China) were cultured in Dulbecco's modified Eagle's medium (DMEM, Gibco, Life Technologies, Carlsbad, CA, USA) supplemented with 10% foetal bovine serum (FBS, Gibco, Life Technologies) and 1% Penicillin/Streptomycin (100 µg/ml, Gibco, Life Technologies) at 37°C with 95% air and 5% CO_2. Cells were incubated with 50 µM hemin for 24 h to establish the ICH cell model.

The shRNA sequences of sh-Lin28, overexpression plasmids oe-Trim37 and their corresponding negative controls were all provided by GenePharma (Shanghai, China). Cell transfection was performed according to the instruction of Lipofectamine 2000 (Invitrogen, instruction of Lipofectamine Carlsbad, CA, USA). Then, transfected cells were placed in the culture medium for 48 h before the subsequent analysis.

Cell counting kit-8 assay

Following the instructions provided by the manufacturer, 1×10^4 HT-22 cells were seeded into 96-well

plates. The 10 µl cell counting kit-8 (CCK-8) solution (Dojindo Molecular Technologies, Inc., Gaithersburg, MA, USA) was added into each well for 2 h-incubation at 37°C 48 h after cell transfection at 24 h, 48 h, 72 h and 96 h. Absorbance at 450 nm was determined using a microplate reader (Thermo Fisher Scientific, Waltham, MA, USA). The experiment of each group was performed in triplicate.

Reverse transcription quantitative polymerase chain reaction (qRT-PCR) assay

The total RNA was derived from brain tissues and mouse hippocampal neurons HT-22 using the TRIzol reagent and synthesized into the complementary DNA using reverse transcription assay kits (R&D SYSTEMS, Inc., Minneapolis, MN, USA). The gene expression was analysed using SYBR Green PCR Master Mix (Thermo Fisher, Shanghai, China). With GAPDH as the endogenous control, qPCR primers are shown in Table I. Real-time quantitative PCR was processed under the following conditions: denaturation at 95°C for 10 min, followed by 40 cycles at 95°C for 15 s, 60°C for 30 s and 72°C for 30 s using Light Cycler 480 (Roche, USA). Relative gene expression was measured based on the $2^{-\Delta\Delta Ct}$ method. The experiment of each group was performed in triplicate.

Enzyme-linked immunosorbent assay

The levels of GSH and ROS were detected strictly following the instructions of GSH and ROS assay kits (R&D SYSTEMS, Inc.). Optical density of each well at 450 nm was determined using a microplate reader and converted to corresponding concentrations according to the standard curve. The experiment of each group was performed in triplicate.

Western blot

The total protein was extracted from brain tissues and HT-22 cells using RIPA lysis buffer (Beyotime Biotechnology, Shanghai, China). Each protein extract (20 µg) was loaded into 12% denatured polyacrylamide gel, followed by transferring into polyvinylidene fluoride membranes (Millipore Co., Ltd., Bedford, MA, USA) for electrophoresis. The membranes were incubated with 5% skim milk at 25°C for 1 h and then with primary antibodies at 4°C overnight. After washing, the membranes were re-incubated with anti-mouse/rabbit secondary antibody of goat IgG H&L (HRP) (ab279647, 1 : 1000, Abcam; ab205718, 1 : 2000, Abcam) at room temperature for 1 h. The immunoreactive bands were detected using the enhanced chemiluminescence system (Amersham Biosciences, Piscataway, NJ, USA) and an electrophoretic image analyser (Bio-Rad, Hemel Hampstead, UK) with GAPDH as the internal reference. The experiment of each group was performed in triplicate. Primary antibodies were used as follows: rabbit monoclonal antibody GPX4 (ab125066, 1 : 1000, Abcam, Cambridge, MA, USA), Lin28A (ab125066, 1 : 1000, Abcam) and mouse monoclonal antibody GAPDH (ab8245, 1 : 500, Abcam).

RNA pull-down assay

The binding of Lin28 and Trim37 was detected using the RAP assay kit. HT-22 cells were lysed using the RNA lysis buffer (Thermo Fisher Scientific), followed by the addition of biotin-labelled RNA. Next, streptavidin beads were cultured with biotin-labelled RNA at 4°C overnight, followed by separation of streptavidin bead-RNA compounds. mRNA level was measured via qRT-PCR.

RNA-binding protein immunoprecipitation (RIP)

The binding of Lin28 and Trim37 was also testified using the RIP assay kits (Millipore Co., Ltd.). HT-22 cells were lysed using RIP lysis buffer. The lysate was cultured with beads conjugated with Argonaute-2 (Ago2, ab186733, 1 : 50, Abcam) or the control IgG (ab6709, 1 : 1000, Abcam). Next, the compound was detached using protease-K and the obtained binding-RNA was analysed using RNA. The experiment of each group was performed in triplicate.

RNA stability analysis

To analyse mRNA decay rate of Trim37 mRNA, cells with a low expression of Lin28 and the control cells were treated with 5 µg/ml actinomycin D to

Table I. qPCR primers

Gene	Forward primer (5'-3')	Reverse primer (5'-3')
Lin28	ATGGGCTCGGTGTCCAACCAGC	TCAATTCTGGGCTTCTGGGAGC
Trim37	GATGAGCAGAGTGTGGAGAGCA	TTACACGTCAGACAGCTGATGG
GAPDH	CTGCCCTTACCCCGGGGTCCC	TTACTCCTTGGAGGCCATGTA

inhibit RNA transcription. The total RNA was extracted from cells at different time points. mRNA level of Trim37 with the addition of actinomycin D at different time points was determined using qRT-PCR with GAPDH as the internal reference. The experiment of each group was performed in triplicate.

Statistical analysis

Data statistical analysis and graphing were processed using SPSS21.0 statistical software (IBM Corp, Armonk, NY, USA) and GraphPad Prism 8.0 software (GraphPad Software Inc., San Diego, CA, USA). Measurement data were presented as mean ± standard deviation (SD) and conformed to normal distribution and homogeneity of variance. Comparisons among various groups were analysed with the help of Student's *t* test and one-way or two-way analysis of variance (ANOVA), followed by data check using Tukey's multiple comparison test. *P* value was calculated by two-tailed tests and $p < 0.05$ indicated statistical significance.

Results

ICH mice exhibited neuronal ferroptosis and upregulation of Lin28 in brain tissues

Intracerebral haemorrhage is diagnosed as a highly risky cerebrovascular disease that triggers a series of parallel pathological processes in brain tissues, leading to secondary brain injury [34]. Ferroptosis is a novel mode of iron-dependent cell programmed death, leading to ICH-induced neuronal damage [1,13]. Previous research has evidenced that Lin28 as an RNA-binding protein is highly expressed in neurons after ICH [5]. Accordingly, we speculated that Lin28 plays a role in neuronal damage after ICH *via* regulating ferroptosis. To probe the regulatory mechanism of Lin28 in neuronal ferroptosis, we first established the ICH mouse model *via* treatment of collagenase VII. After modelling, neurological functions of mice were assessed and we found that neurological function deficit scores were markedly increased and forelimb placing and corner turn tests both indicated the impairment of neurological functions in the model mice ($p < 0.05$, Fig. 1A). Then, we measured the cerebral oedema and hematoma volume. The results showed that brain tissues in the model mice were presented with augmented water content ($p < 0.05$, Fig. 1B) and obvious hematoma ($p < 0.05$, Fig. 1C). Histopathological changes of brain tissues were observed using H&E staining, which observed that post-ICH, brain tissues exhibited obvious oedema, partial neuronal necrosis, glial cell swelling, intracellular vacuoles and noticeable inflammatory cell infiltration (Fig. 1D). To further analyse the impact of ICH on neuronal ferroptosis, we detected the level of ferroptosis-related factors. The results showed that Fe^{2+} concentration in brain tissues and ROS activity in the serum ($p < 0.05$, Fig. 1E, F) were significantly elevated, while GSH content in the serum ($p < 0.05$, Fig. 1G) and GPX4 expression in brain tissues ($p < 0.05$, Fig. 1I) were significantly reduced in ICH mice. At last, we detected Lin28 expression and found that Lin28 was highly expressed in brain tissues of ICH mice ($p < 0.05$, Fig. 1H, I). The above results indicated that ICH induced neuronal ferroptosis and Lin28 was highly expressed in ICH mice.

Lin28 inhibition suppressed neuronal ferroptosis and brain injury in ICH mice

To explore the role of Lin28 in regulating neuronal ferroptosis, we first injected lentivirus vectors (LV-sh-Lin28 or LV-sh-NC) into mouse right hippocampus to inhibit Lin28 expression ($p < 0.05$, Fig. 2A, B). Then, we assessed mouse neurological function deficit, oedema and hematoma, and found that Lin28 inhibition reversed ICH induced-neurological impairment to some extent ($p < 0.05$, Fig. 2C) with alleviation of cerebral oedema and hematoma ($p < 0.05$, Fig. 2D, E). Besides, H&E staining showed that Lin28 inhibition alleviated oedema, hematoma, neuronal necrosis, glial cell swelling, intracellular vacuoles and inflammatory cell infiltration in brain tissues ($p < 0.05$, Fig. 2F). Moreover, ROS activity in the serum was diminished ($p < 0.05$, Fig. 2G), GSH content in the serum ($p < 0.05$, Fig. 2H) and GPX4 expression in brain tissues ($p < 0.05$, Fig. 2B) were increased, and Fe^{2+} concentration was reduced ($p < 0.05$, Fig. 2I) in brain tissues upon Lin28 inhibition. In brief, Lin28 inhibition could suppress neuronal ferroptosis and alleviate brain injury in ICH mice.

Silencing Lin28 attenuated ICH-induced neuronal ferroptosis of HT-22 cells *in vitro*

To confirm the regulatory role of Lin28 in ICH-induced neuronal ferroptosis in vitro, we induced HT-22 cells using hemin treatment to establish the

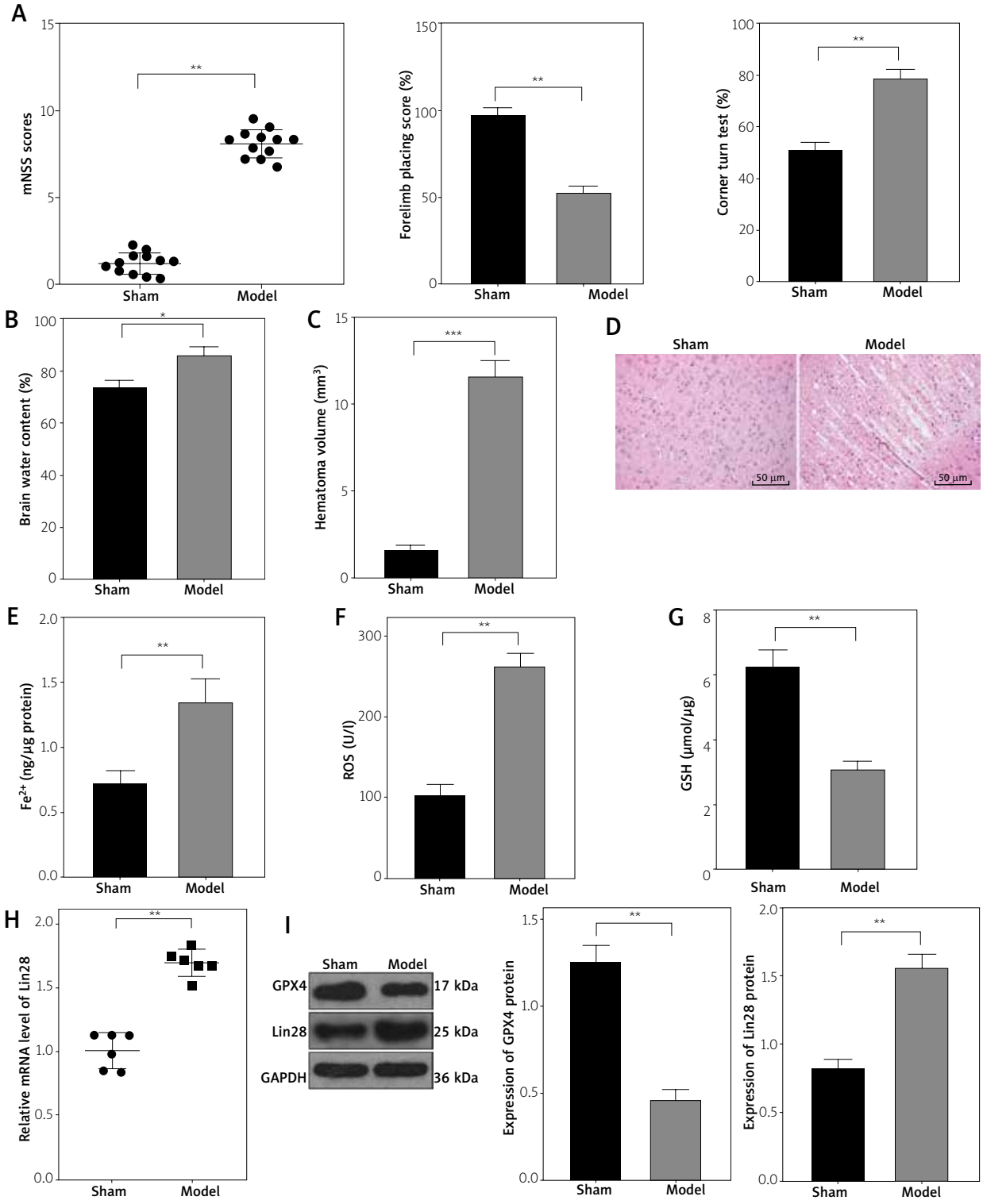

Fig. 1. Intracerebral haemorrhage (ICH) mice exhibited neuronal ferroptosis and upregulation of Lin28 in brain tissues. The ICH mouse model was established using treatment of collagenase VII. **A**) Neurological function deficit score (the score was from 0 to 18 with a higher score indicating more severe neurological impairment), forelimb placing test (the success rate of mouse forelimb placing on the table) and corner turn test (percentage of left turn to get out of the corner) to assess mouse neurological functions, $n = 12$; **B**) Cerebral oedema; **C**) Cerebral hematoma; **D**) Histopathological changes of brain tissues observed *via* H&E staining; **E**) Relative concentration of Fe^{2+} detected *via* the iron content assay kit; **F-G**) ROS and GSH activity in the serum detected *via* ELISA; **H**) mRNA level of Lin28 in brain tissues detected *via* qRT-PCR; **I**) Protein expressions of GPX4 and Lin28 detected *via* western blot; $n = 6$, data were presented as mean ± SD and analysed using Student's *t* test. After analysis, data were checked by Tukey's multiple comparison test. $^*p < 0.05$, $^{**}p < 0.01$, $^{***}p < 0.001$.

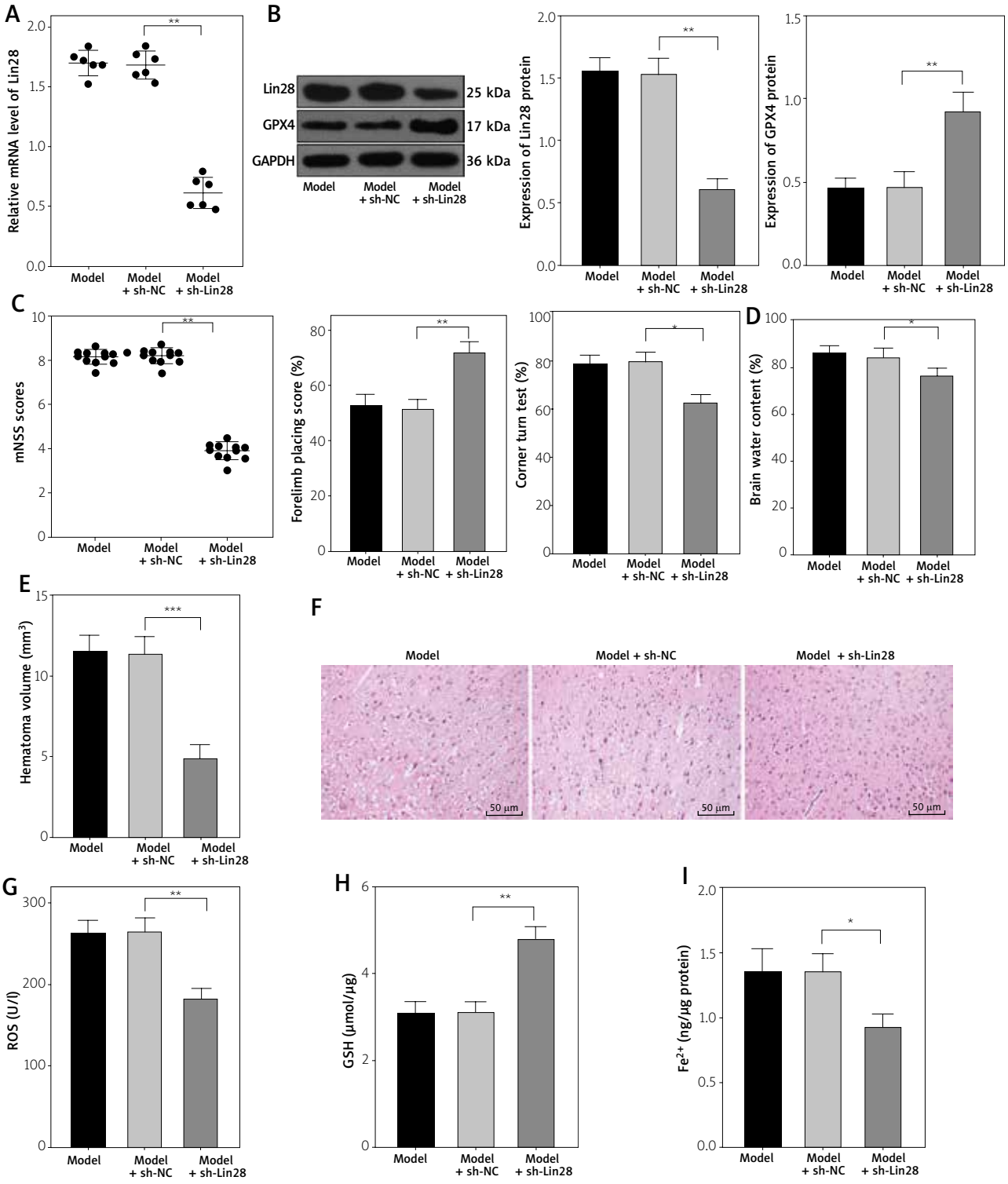

Fig. 2. Lin28 inhibition suppressed neuronal ferroptosis and brain injury in intracerebral haemorrhage (ICH) mice. Lin28 expression was inhibited *via* injection of lentivirus vectors (LV-sh-Lin28 or LV-sh-NC) into mouse hippocampus. **A**) mRNA level of Lin28 in brain tissues verified *via* qRT-PCR; **B**) Protein expressions of Lin28 and GPX4 in brain tissues detected *via* western bot; **C**) Neurological function deficit score (the score was from 0 to 18 with a higher score indicating more severe neurological impairment), forelimb placing test (the success rate of mouse forelimb placing on the table) and corner turn test (percentage of left turn to get out of the corner) to assess mouse neurological functions, $n = 12$; **D**) Cerebral oedema; **E**) Cerebral hematoma; **F**) Histopathological changes of brain tissues observed *via* H&E staining; **G, H**) ROS and GSH contents in the serum detected *via* ELISA; **I**) Relative concentration of Fe^{2+} detected *via* the iron content assay kit. $n = 6$, data were presented as mean ± SD and analysed using one-way ANOVA. After analysis, data were checked by Tukey's multiple comparison test. $^{*}p < 0.05$, $^{**}p < 0.01$, $^{***}p < 0.001$.

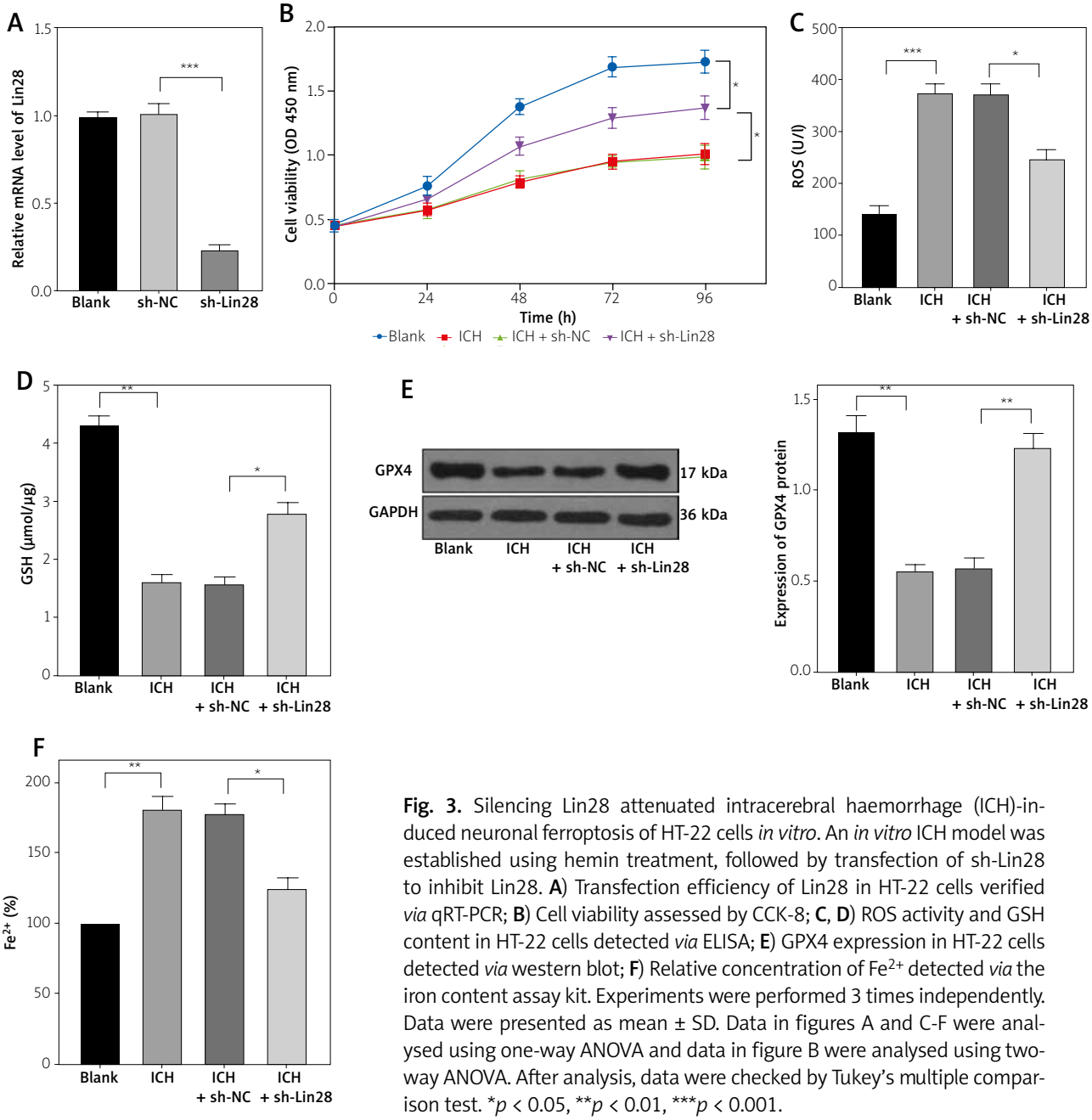

Fig. 3. Silencing Lin28 attenuated intracerebral haemorrhage (ICH)-induced neuronal ferroptosis of HT-22 cells *in vitro*. An *in vitro* ICH model was established using hemin treatment, followed by transfection of sh-Lin28 to inhibit Lin28. **A**) Transfection efficiency of Lin28 in HT-22 cells verified *via* qRT-PCR; **B**) Cell viability assessed by CCK-8; **C**, **D**) ROS activity and GSH content in HT-22 cells detected *via* ELISA; **E**) GPX4 expression in HT-22 cells detected *via* western blot; **F**) Relative concentration of Fe^{2+} detected *via* the iron content assay kit. Experiments were performed 3 times independently. Data were presented as mean ± SD. Data in figures A and C-F were analysed using one-way ANOVA and data in figure B were analysed using two-way ANOVA. After analysis, data were checked by Tukey's multiple comparison test. *$p < 0.05$, **$p < 0.01$, ***$p < 0.001$.

in vitro ICH model. After induction, HT-22 cells were transfected with sh-Lin28 to silence Lin28 expression ($p < 0.05$, Fig. 3A). After silencing Lin28, cell viability was enhanced ($p < 0.05$, Fig. 3B) and the changes of ROS activity, GSH content, GPX4 expression and Fe^{2+} concentration caused by hemin treatment were reversed ($p < 0.05$, Fig. 3F). Collectively, Lin28 could alleviate ICH-induced ferroptosis in both mouse brain tissues and neurons.

Lin28 bound to Trim37 mRNA to stabilize the mRNA level of Trim37

Prior works shed light on the function of RBP on regulation of mRNA stability in the nervous system *via* binding to its targets [23]. However, whether ICH-induced neuronal ferroptosis is affected by this mechanism remains unknown. Lin28 as a RBP could modulate mRNA stability of its target genes [18]. Besides, Trim37 mRNA was highly expressed in ICH [8].

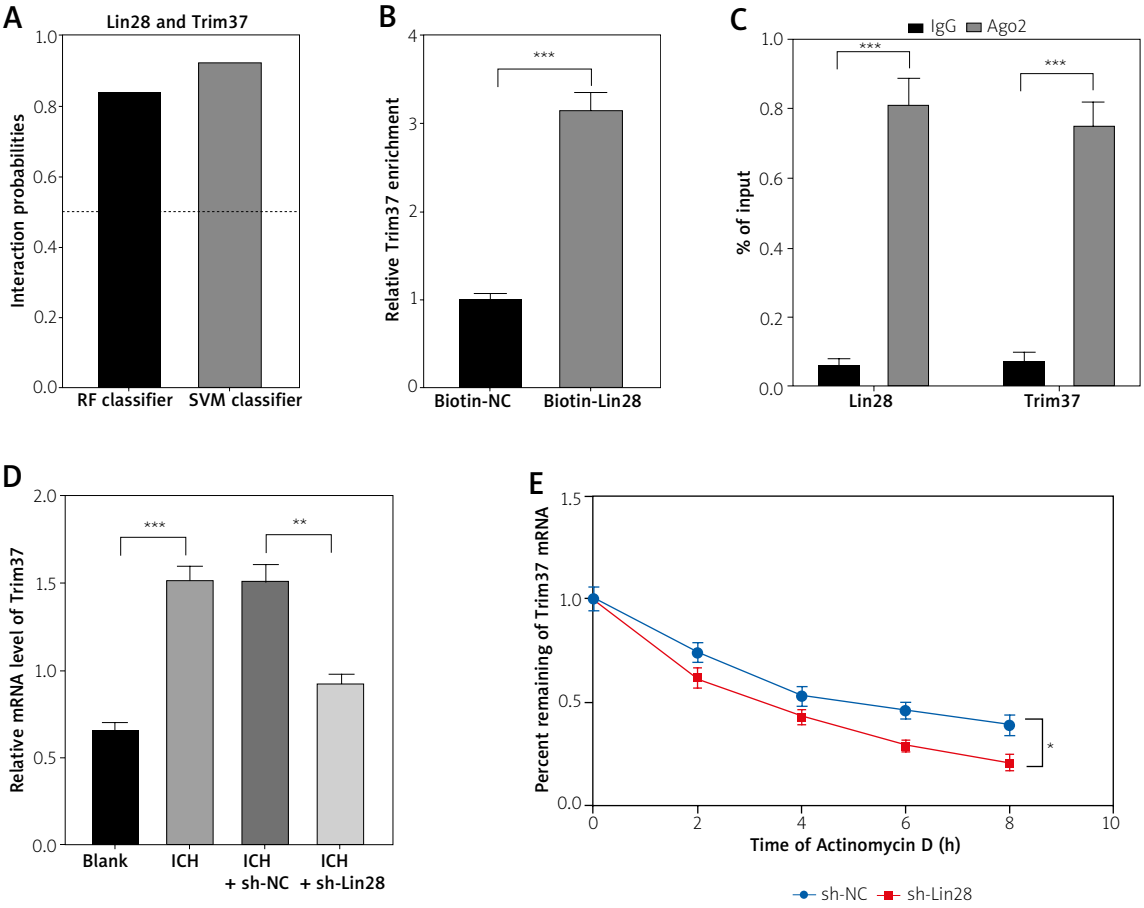

Fig. 4. Lin28 bound to Trim37 mRNA to stabilize the mRNA level of Trim37. **A**) Binding of Lin28a and Trim37 mRNA analysed *via* the RNA-protein binding prediction website (http://pridb.gdcb.iastate.edu/RPISeq/); **B, C**) Binding of Lin28a and Trim37 mRNA verified *via* RNA pull-down and RIP assays; **D**) Transcription level of Trim37 in sh-Lin28-transfetced HT-22 cells detected *via* qRT-PCR; **E**) mRNA level of Trim37 in actinomycin-D-treated HT-22 cell at different times. Experiments were performed 3 times independently. Data were presented as mean ± SD. Data in figure B was analysed using Student's *t* test, data in figure D were analysed using one-way ANOVA and data in figures C and E were analysed using two-way ANOVA. After analysis, data were checked by Tukey's multiple comparison test. *$p < 0.05$, **$p < 0.01$, ***$p < 0.001$.

Presumably, Lin28 could bind to Trim37 mRNA to regulate the stability of Trim37 mRNA. RNA-protein binding prediction website (http://pridb.gdcb.iastate.edu/RPISeq/) indicated that Lin28 is likely to bind to Trim37 mRNA ($p < 0.05$, Fig. 4A). The binding of Lin28 and Trim37 mRNA was further verified via RNA pull-down and RIP assays ($p < 0.05$, Fig. 4B, C). Subsequently, we detected the mRNA level of Trim37 in sh-Lin28-transfected HT-22 cells and noted that Trim37 expression in HT-22 cells were downregulated upon Lin28 inhibition ($p < 0.05$, Fig. 4D). Finally, we analysed the stability of Trim37 mRNA and found that Trim37 stability in HT-22 cells was significantly weakened after silencing Lin28 ($p < 0.05$, Fig. 4E). Taken together, Lin28 could bind to Trim37 mRNA to stabilize the mRNA level of Trim37.

Overexpression of Trim37 reversed the alleviating role of silencing Lin28 in neuronal ferroptosis after ICH

To further investigate the regulatory role of Trim37 in Lin28-mediated neuronal ferroptosis after ICH, HT-22 cells were transfected with oe-Trim37 to upregulate Trim37 ($p < 0.05$, Fig. 5A), followed by transfec-

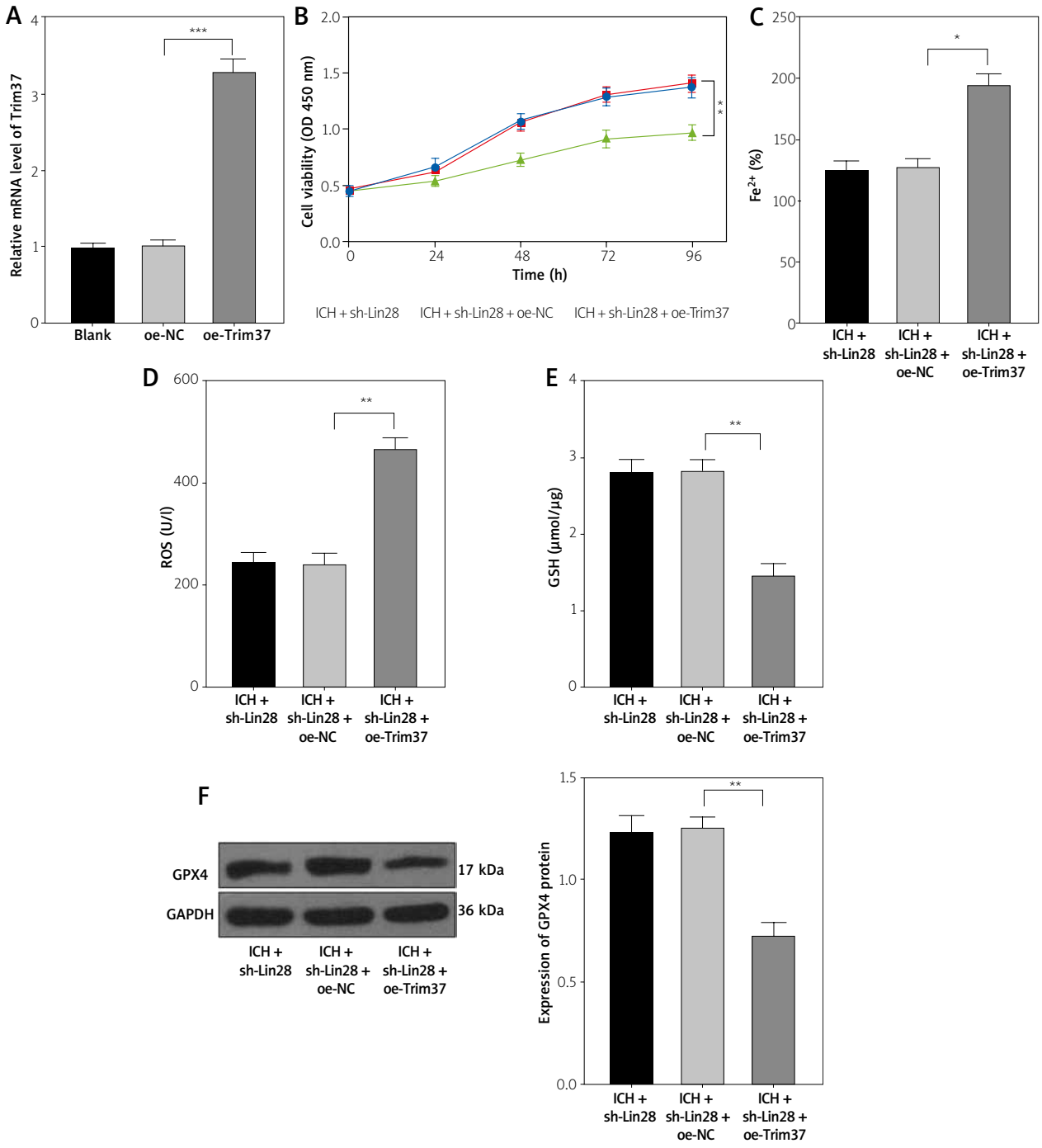

Fig. 5. Overexpression of Trim37 reversed the alleviating role of silencing Lin28 in neuronal ferroptosis after intracerebral haemorrhage (ICH). Hemin-induced HT-22 cells were transfected with oe-Trim37 to elevate Trim37 expression. **A**) Transfection efficiency of Trim37 in HT-22 cells detected *via* qRT-PCR; **B**) CCK-8 viability assessed *via* CCK-8; **C**) Relative concentration of Fe^{2+} detected *via* the iron content assay kit; **D, E**) ROS and GSH contents detected *via* ELISA; **F**) GPX4 expression analysed *via* western blot. Experiments were performed 3 times independently. Data were presented as mean ± SD. Data in figures A, and C-F were analysed using one-way ANOVA and data in figure B were analysed using two-way ANOVA. After analysis, data were checked by Tukey's multiple comparison test. *$p < 0.05$, **$p < 0.01$, ***$p < 0.001$.

tion of sh-Lin28. Our results showed that cell viability was significantly reduced ($p < 0.05$, Fig. 5B) and Fe^{+} content was markedly increased ($p < 0.05$, Fig. 5C) upon Trim37 overexpression, and Trim37 overexpression reversed the changes of ROS, GSH contents and GPX4 expression caused by silencing Lin28 ($p < 0.05$, Fig. 5D-F). Overall, Lin28 could stabilize the mRNA level of Trim37 *via* binding to Trim37 mRNA, thus promoting neuronal ferroptosis after ICH.

Discussion

Intracerebral haemorrhage is a common cerebrovascular disease with poor prognosis [22]. Neuronal ferroptosis is an essential mechanism in aggravation of symptoms after ICH [1]. Lin28 as an RBP, is aberrantly expressed in neurons after ICH and promotes astrocytic proliferation to regulate neuronal injury [5]. However, the regulatory mechanism of Lin28 in ICH has not been discussed before. In this study, we highlighted that Lin28 plays a role in neuronal ferroptosis *via* regulation of Trim37 mRNA stability after ICH.

Oestrogen was previously reported to influence ICH-induced brain injury [20,30]. To minimize possible interference to the experimental results, we just selected male mice to establish the ICH mouse model by injection of collagenase VII. After modelling, neurological function deficit scores, forelimb placing and corner turn tests indicated that mice exhibited significant neurological impairment. Besides, brain tissues of ICH mice were pathologically presented with obvious hematoma and oedema, neuronal necrosis, glial cell swelling, intracellular vacuoles and inflammatory cell infiltration. Prior studies have shed light on the protecting role of limiting neuronal ferroptosis in the haemorrhagic brain [17,26]. ROS (a by-product of mitochondrial metabolism) and Fe^{2+} (redox-active transition metal) are essential for induction of ferroptosis, while GPX4 and GSH are critical antioxidants to counteract the release of ROS and Fe^{2+} [6,24]. ROS activity and Fe^{2+} concentration were increased, while GPX4 and GSH levels were decreased in brain tissues of ICH mice. Besides, our experiments showed that Lin28 was increased in brain tissues of ICH mice. Lin28 was reported to have an upregulation in neurons after ICH [5]. Next, we silenced Lin28 expression in ICH mice *via* injection of LV-sh-Lin28 in mouse right hippocampus. Upon Lin28 upregulation, neurological impairment, oedema and hematoma volume, and histopathological changes of ICH mice were attenuated. Moreover, Lin28 upregulation also reversed ICH-induced changes of ROS, Fe^{2+}, GPX4 and GSH. Consistently, Lin28 overexpression induces neurite underdevelopment, thus impaired neurological functions [12]. On top of that, an *in vitro* ICH model was established using hemin to induce HT-22 cells, followed by silencing Lin28. Silencing Lin28 led to elevated cell viability with increased GSH content and GPX4 expression and decreased ROS activity and Fe^{2+} concentration. Lin28 downregulation rescues bupivacaine-induced neuronal apoptosis, while Lin28 upregulation plays an opposite role [31]. Similarly, depletion of Lin28 enhances cell viability while it inhibits apoptosis of human umbilical vein endothelial cells in high-glucose conditions [32]. Admittedly, the role of Lin28 in ferroptosis has not been reported before, and we initially demonstrated that silencing Lin28 plays an alleviating role in neuronal ferroptosis after ICH *in vivo* and *in vitro*.

Lin28 has been previously evidenced to bind to Trim proteins, such as Trim-71 [25]. Trim37 was highly expressed in the serum of ICH patients and associated with apoptosis of microglia in ICH [8]. In clinical settings, patients with a high level of Trim37 displayed slightly neurological function deficits [15]. The database predicted that Lin28 could bind to Trim37 mRNA, which was in line with the results of RNA pull-down and RIP assays. Trim37 was markedly decreased in HT-22 cells with low expression of HT-22. Besides, mRNA of Trim37 was destabilized upon Lin28 inhibition. Collectively, Lin28 could bind to Trim37 mRNA to stabilize mRNA level of Trim37. Our subsequent experimentation showed that overexpression of Trim37 in sh-Lin28-treated HT-22 cells reduced cell viability with augmented Fe^{+} content, ROS activity and diminished GSH content and GPX4 expression. In line of this, Trim37 inhibition was illustrated to counteract inflammatory injury and apoptosis in human pulmonary alveolar epithelial cells and human embryonic lung fibroblasts in pulmonary inflammation and acute lung injury [4,28]. Altogether, overexpression of Trim37 abolished the alleviating role of silencing Lin28 in neuronal ferroptosis after ICH.

In summary, our findings uncovered that Lin28 could bind to Trim37 mRNA to stabilize the mRNA level of Trim37, thereby promoting neuronal ferroptosis after ICH *in vivo* and *in vitro*. This study was the first to evaluate the regulatory mechanism of Lin28 in neuronal ferroptosis after ICH and hinted

a novel therapeutic target of ICH. Nonetheless, this study failed to explore the role of Lin28 in other modes of cell death, such as apoptosis and pyroptosis, and potential effects of other targets of Lin28 in neural ferroptosis, except Trim37. Moreover, this study is insufficient to validate the role of Trim37 in animals. The role of the Lin28-mediated Trim37 axis in other modes of neuronal death, other targets of Lin28 in ICH, effect of Trim37 in ICH animal models and whether Trim37 could regulate protein ubiquitination level to affect neuronal ferroptosis post-ICH remain to be further investigated with future endeavours.

Acknowledgements

This research was supported by the Natural Science Foundation of China (81971126) and the Guizhou Science and Technology Foundation No: Qiankehe support [2021] general (071).

Ethics statement

The animal experimentation is conducted in accordance with the protocol approved by the animal ethics committee of the Guizhou Medical University, and strictly followed the Guidelines for the Care and Use of Laboratory Animals [14].

Disclosure

The authors report no conflict of interest.

References

1. Bai Q, Liu J, Wang G. Ferroptosis, a regulated neuronal cell death type after intracerebral hemorrhage. Front Cell Neurosci 2020; 14: 591874.
2. Bai X, Zhang YL, Liu LN. Inhibition of TRIM8 restrains ischaemia-reperfusion-mediated cerebral injury by regulation of NF-kappaB activation associated inflammation and apoptosis. Exp Cell Res 2020; 388: 111818.
3. Bhuiyan MIH, Kim SY, Cho KO. Lin28 overexpression inhibits neurite outgrowth of primary cortical neurons in vitro. Acta Neurobiol Exp (Wars) 2018; 78: 297-304.
4. Chen C, Zhang H, Ge M, Ye J, Li R, Wang D. LncRNA NEAT1 acts as a key regulator of cell apoptosis and inflammatory response by the miR-944/TRIM37 axis in acute lung injury. J Pharmacol Sci 2021; 145: 202-212.
5. Ding W, Wang Y, Cheng Y, Chen X, Chen W, Zuo P, Chen W, Qiao Z, Fan X. Lin28 is associated with astrocytic proliferation during intracerebral hemorrhage. Int J Clin Exp Pathol 2020; 13: 1136-1145.
6. Forcina GC, Dixon SJ. GPX4 at the crossroads of lipid homeostasis and ferroptosis. Proteomics 2019; 19: e1800311.
7. Garg R, Biller J. Recent advances in spontaneous intracerebral hemorrhage. F1000Res 2019; 8: F1000 Faculty Rev-302.
8. Han C, Xia X, Jiao S, Li G, Ran Q, Yao S. Tripartite motif containing protein 37 involves in thrombin stimulated BV-2 microglial cell apoptosis and interleukin 1beta release. Biochem Biophys Res Commun 2019; 516: 1252-1257.
9. Hao MQ, Xie LJ, Leng W, Xue RW. Trim47 is a critical regulator of cerebral ischemia-reperfusion injury through regulating apoptosis and inflammation. Biochem Biophys Res Commun 2019; 515: 651-657.
10. Hatakeyama S. TRIM family proteins: roles in autophagy, immunity, and carcinogenesis. Trends Biochem Sci 2017; 42: 297-311.
11. Ironside N, Chen CJ, Ding D, Mayer SA, Connolly ES, Jr. Perihematomal edema after spontaneous intracerebral hemorrhage. Stroke 2019; 50: 1626-1633.
12. Jang HJ, Kim JY, Kim SY, Cho KO. Persistent Lin28 expression impairs neurite outgrowth and cognitive function in the developing mouse neocortex. Mol Neurobiol 2019; 56: 3780-3795.
13. Jin Y, Zhuang Y, Liu M, Che J, Dong X. Inhibiting ferroptosis: A novel approach for stroke therapeutics. Drug Discov Today 2021; 26: 916-930.
14. Jones-Bolin S. Guidelines for the care and use of laboratory animals in biomedical research. Curr Protoc Pharmacol 2012; Appendix 4: Appendix 4B.
15. Kallijarvi J, Hamalainen RH, Karlberg N, Sainio K, Lehesjoki AE. Tissue expression of the mulibrey nanism-associated Trim37 protein in embryonic and adult mouse tissues. Histochem Cell Biol 2006; 126: 325-334.
16. Li C, Sako Y, Imai A, Nishiyama T, Thompson K, Kubo M, Hiwatashi Y, Kabeya Y, Karlson D, Wu SH, Ishikawa M, Murata T, Benfey PN, Sato Y, Tamada Y, Hasebe M. A Lin28 homologue reprograms differentiated cells to stem cells in the moss Physcomitrella patens. Nat Commun 2017; 8: 14242.
17. Li Q, Han X, Lan X, Gao Y, Wan J, Durham F, Cheng T, Yang J, Wang Z, Jiang C, Ying M, Koehler RC, Stockwell BR, Wang J. Inhibition of neuronal ferroptosis protects hemorrhagic brain. JCI Insight 2017; 2: e90777.
18. Mayr F, Heinemann U. Mechanisms of Lin28-mediated miRNA and mRNA regulation--a structural and functional perspective. Int J Mol Sci 2013; 14: 16532-16553.
19. Menendez-Pelaez A, Santana C, Howes KA, Sabry I, Reiter RJ. Effects of photoperiod or exogenous melatonin administration on the activity of N-acetyltransferase and hydroxyindole-O-methyltransferase and the melatonin content of the harderian gland of two strains of female Syrian hamsters. J Pineal Res 1988; 5: 293-300.
20. Nakamura T, Xi G, Hua Y, Schallert T, Hoff JT, Keep RF. Intracerebral hemorrhage in mice: model characterization and application for genetically modified mice. J Cereb Blood Flow Metab 2004; 24: 487-494.
21. Ni SY, Xu WT, Liao GY, Wang YL, Li J. LncRNA HOTAIR Promotes LPS-induced inflammation and apoptosis of cardiomyocytes via Lin28-mediated PDCD4 stability. Inflammation 2021; 44: 1452-1463.
22. Parry-Jones AR, Paley L, Bray BD, Hoffman AM, James M, Cloud GC, Tyrrell PJ, Rudd AG, Group SC. Care-limiting decisions in acute

stroke and association with survival: analyses of UK national quality register data. Int J Stroke 2016; 11: 321-331.
23. Prashad S, Gopal PP. RNA-binding proteins in neurological development and disease. RNA Biol 2021; 18: 972-987.
24. Tang D, Chen X, Kang R, Kroemer G. Ferroptosis: molecular mechanisms and health implications. Cell Res 2021; 31: 107-125.
25. Treiber T, Treiber N, Plessmann U, Harlander S, Daiss JL, Eichner N, Lehmann G, Schall K, Urlaub H, Meister G. A Compendium of RNA-binding proteins that regulate microRNA biogenesis. Mol Cell 2017; 66: 270-284.e13.
26. Wan J, Ren H, Wang J. Iron toxicity, lipid peroxidation and ferroptosis after intracerebral haemorrhage. Stroke Vasc Neurol 2019; 4: 93-95.
27. Wu X, Luo J, Liu H, Cui W, Guo W, Zhao L, Guo H, Bai H, Guo K, Feng D, Qu Y. Recombinant adiponectin peptide promotes neuronal survival after intracerebral haemorrhage by suppressing mitochondrial and ATF4-CHOP apoptosis pathways in diabetic mice via Smad3 signalling inhibition. Cell Prolif 2020; 53: e12759.
28. Xiang Y, Zhang S, Lu J, Zhang W, Cai M, Xiang J, Cai D. Ginkgolide B protects human pulmonary alveolar epithelial A549 cells from lipopolysaccharide-induced inflammatory responses by reducing TRIM37-mediated NF-kappaB activation. Biotechnol Appl Biochem 2020; 67: 903-911.
29. Xie X, Wang F, Li X. Inhibition of TRIM14 protects cerebral ischemia/reperfusion injury through regulating NF-kappaB/NLRP3 pathway-mediated inflammation and apoptosis. J Recept Signal Transduct Res 2021; 10: 1-9.
30. Xie Y, Li YJ, Lei B, Kernagis D, Liu WW, Bennett ER, Venkatraman T, Lascola CD, Laskowitz DT, Warner DS, James ML. Sex Differences in Gene and Protein Expression After Intracerebral Hemorrhage in Mice. Transl Stroke Res 2019; 10: 231-239.
31. Yu L, Jiang Y, Tang B. Lin28a functionally modulates bupivacaine-induced dorsal root ganglion neuron apoptosis through TrkA activation. Biomed Pharmacother 2018; 98: 63-68.
32. Zhang W, Sui Y. CircBPTF knockdown ameliorates high glucose-induced inflammatory injuries and oxidative stress by targeting the miR-384/LIN28B axis in human umbilical vein endothelial cells. Mol Cell Biochem 2020; 471: 101-111.
33. Zhang Y, Rui T, Luo C, Li Q. Mdivi-1 alleviates brain damage and synaptic dysfunction after intracerebral hemorrhage in mice. Exp Brain Res 2021; 239: 1581-1593.
34. Zhu H, Wang Z, Yu J, Yang X, He F, Liu Z, Che F, Chen X, Ren H, Hong M, Wang J. Role and mechanisms of cytokines in the secondary brain injury after intracerebral hemorrhage. Prog Neurobiol 2019; 178: 101610.
35. Ziai WC, Carhuapoma JR. Intracerebral hemorrhage. Continuum (Minneap Minn) 2018; 24: 1603-1622.